Effects of liquefaction-modified ground motions on building fragility curves

W. Zhan [(1)], L. G. Baise [(2)], Q. Chen [(3)], C. H. Juang [(4)] , F. Miao [(5)]

[(1)] *Postdoctoral Scholar, Civil and Environmental Engineering Department, Tufts University, Medford, MA, USA* weiwei.zhan@tufts.edu

[(2)] *Professor, Civil and Environmental Engineering Department, Tufts University, Medford, MA, USA* laurie.baise@tufts.edu

[(3)] *Associated Professor, Glenn Department of Civil Engineering, Clemson University, Clemson, SC, USA,* qiushi@clemson.edu

[(4)] *Professor, Department and Civil Engineering and Graduate Institute of Applied Geology, National Central University, Taoyuan, Taiwan,* hsein@clemson.edu

[(5)] *Associate Professor, Faculty of Engineering, China University of Geosciences, Wuhan, China,* fsmiao@cug.edu.cn

Abstract

Earthquake-induced liquefaction is one of the leading causes of seismic damage, especially in urban cities located on young deposits or reclaimed lands. Liquefaction could impose two types of demands influencing seismic performance of structures: excessive ground deformations and unfavorable ground motions. Liquefaction-modified ground motions are characterized by a characteristic waveform of high-frequency acceleration spikes riding on a low-frequency carrier, showing distinct frequency characteristics to non-liquefaction-modified ground motions. To advance the performance-based earthquake engineering practices for buildings at liquefiable sites, we introduce a framework to quantify the effects of liquefaction-modified ground motions on the seismic fragility of buildings. For this goal, a four-story steel moment-resisting frame building used in the 2007 E-Defense full-scale shaking table test is selected as a case building prototype. Incremental dynamic analyses are conducted to determine the seismic fragility curves of the building prototype subjected to the 344 ground motion records divided into three groups: liquefaction-modified, non-liquefaction-modified, and all ground motions. Three sets of fragility curves are derived using the peak ground acceleration as the intensity measure and the maximum peak inter-story drift ratio as the damage measure. The results suggest the selected building is more vulnerable to the liquefaction-modified ground motions. The liquefaction-modified ground motions could increase the probability of exceeding collapse and immediate occupancy damage states by up to 2.5 and 2 times, respectively. The structure fragility is adversely affected by the enhancement of long-period ground motion due to liquefaction-induced softening. Future studies will need to investigate liquefaction effects on different types of buildings and explore other intensity measures such as pseudo-spectral acceleration and peak ground velocity for the fragility analysis.

Keywords: fragility curves; steel frame; incremental dynamic analysis; liquefaction effects; ground motions

1. Introduction

Earthquake-induced ground failure hazards such as soil liquefaction can cause notable damage compared with the seismic shaking hazard [1]. Recent major earthquakes, such as the 2011 Mw 9.0 Tohoku earthquake [2] and the 2010-2011 Canterbury Earthquake Sequence (CES) [3], revealed that soil liquefaction could be a significant contributor to earthquake damage in urban areas. For instance, during 2010-2011 CES, liquefaction affected nearly 60,000 residential buildings, many multi-story buildings in the central business district, and the infrastructure system over approximately one-third of the Canterbury city area, accounting for approximately half of the NZD 30 billion loss [3]. Despite research efforts on assessing the likelihood and severity of liquefaction hazard [4],[5] and mechanisms of liquefaction-induced building deformation [6], a full understanding on how liquefaction will impact the seismic performance of structures such as buildings is less well understood.

For seismic performance assessment, soil liquefaction can generate two types of demands on the structure: (1) excessive ground deformation demand; and (2) modified seismic acceleration demand. While liquefaction-induced ground deformation has been extensively studied for both free-field and building environments [6][7], the effect of the modified acceleration demand on the seismic performance of buildings is not yet well understood. Seismic observations from liquefied ground motion stations have revealed that the acceleration time histories of liquefaction-modified ground motions have a characteristic waveform composed of intermittent high-frequency acceleration spikes riding on a low-frequency carrier (see Fig. 1) [8]~[11]. Through comparing the pseudo-spectral acceleration spectrum, previous studies found that soil liquefaction tends to amplify the long-period spectral accelerations (with periods exceeding 1.0 second) as the soil softening induced by soil liquefaction can lengthen the site fundamental period [12][13]. Nevertheless, the effects of liquefaction-modified ground motions on buildings' seismic performance have not been studied.

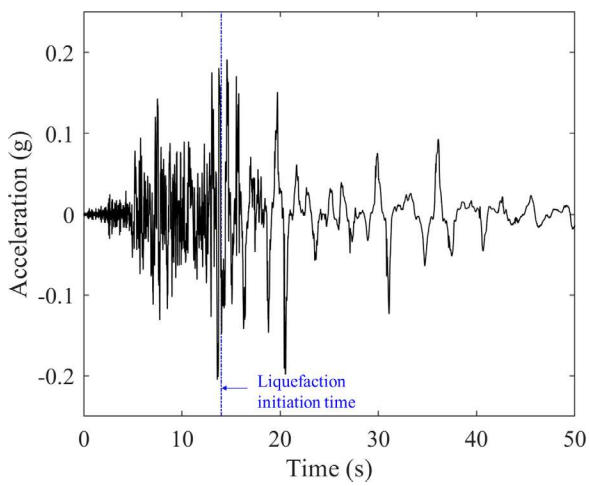

Fig. 1 An example waveform showing liquefaction-modification effects on ground motions. The time history data is recorded by the Wildlife Liquefaction Array during the 1987 Superstition Hills earthquake

In this work, the effects of liquefaction-modified ground motions on buildings' seismic performance are investigated through probabilistic seismic fragility analyses. A worldwide ground motion dataset labeled with liquefaction observation near the ground motion stations was previously compiled for the accelerogram-based liquefaction detection purpose [14]. In total, 344 ground motions from both nonliquefied and liquefied stations (described in Section 2) are selected as input ground motions for the structural dynamic analysis. One four-story steel moment-resisting frame structure designed based on Japanese seismic provisions and tested on the E-Defense Full-Scale Shake Table has been selected as the case building. Its design characteristics are described in Section 3. The numerical model of the selected structure and its validation in

terms of the seismic performance are shown in Section 4. The methods and results of the fragility analysis and incremental dynamic analysis are presented in Section 5, and the last section draws the main conclusions.

2. Ground motion selection

In the first author's dissertation work [15], a worldwide ground motion dataset was compiled to develop a new accelerogram-based method for the quick assessment of liquefaction occurrence [14]. This dataset includes the three-component ground motion records and the associated liquefaction observations from 167 ground motion stations. Among them, 32 stations were liquefied ("LQ"), and the other 135 stations were non-liquefied ("NonLQ"). Since the ground motion stations are usually not installed on liquefiable sites and the liquefaction occurrence requires relatively strict triggering conditions, the liquefaction-modified ground motions are minimal across the globe. The number of the liquefaction-modified ground motions in that dataset [15] is more than several similar datasets [2],[13][16]. The previous study [15] has shown that the liquefaction could significantly modify the frequency parameters of ground motions, which can be applied to detect the subsoil liquefaction based on the surface accelerograms. This works will extend the dataset to investigate the influence of liquefaction-modified ground motions on seismic fragility assessment of buildings.

Each horizontal component of the 167 pairs of ground motions is used individually as the input ground motion for the structural dynamic analysis of the two-dimensional numerical structure model. Hence, the number of LQ and NonLQ ground motions is 64 and 270, respectively. Their peak ground acceleration (PGA) ranges from 0.03 to 1.78 g. The average value and standard deviation of the PGA are 0.29 and 0.22 g. Their 5%-damped pseudo-spectral acceleration (PSA) curves are shown in Fig. 2(a). The averaged PSA curve and its variation of the LQ and NonLQ ground motions are shown in Fig. 2(b). The results suggest that the LQ ground motions have larger average PSA values than the NonLQ ground motion when the period exceeds about 0.3 seconds. The LQ records have large PSA values (i.e., relatively flat PSA curve) and large variance at the period range of 0.3~ 1.3 seconds. This analysis confirms that liquefaction tends to influence the long-period PSA values, as suggested in previous studies [12][13]. The influence of these period-related changes on buildings' seismic performances will be examined using detailed nonlinear dynamic time-history analyses described in Sections 4 and 5.

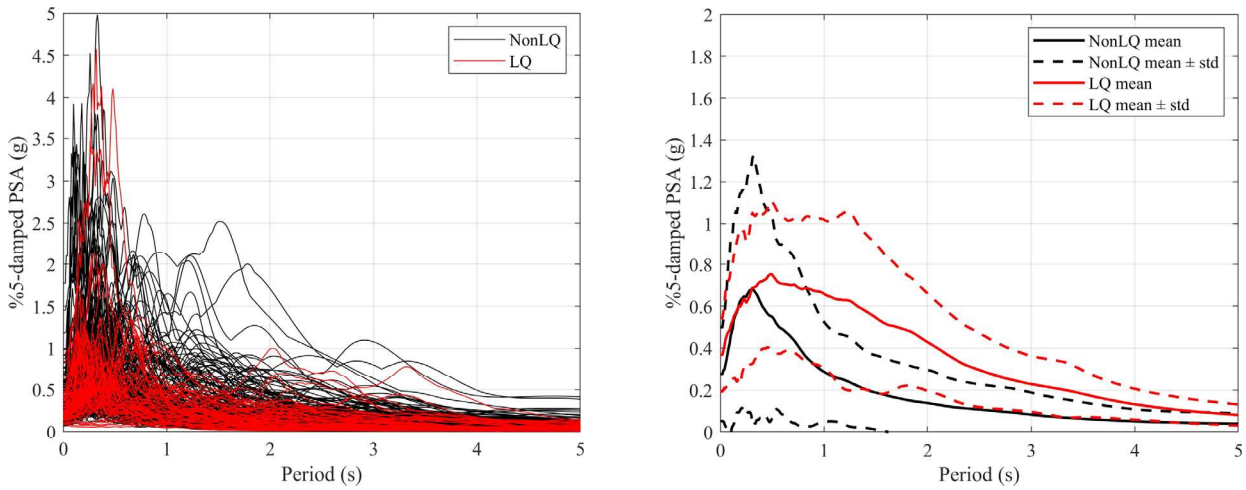

(a) (b)

Fig. 2 The 5%-damped pseudo-spectral acceleration of the selected ground motions: (a) raw PSA curves; (b) mean and standard deviation values of the PSA curves

3. Description of the selected building

A two-by-one bay, four-story steel moment-resisting frame structure is selected as a case building to investigate the effects of liquefaction-modification ground motions on the seismic performance of buildings. The geometry of the structure is 10 and 6 m in the longitudinal (Y) and transverse directions (X), respectively (Fig. 3a). Each story's height is 3.5 m except for the first story, which is 3.875 m (Fig. 3b). The structure was designed based on the Japanese seismic provisions [17],[18]. The steel columns are 300×9 hollow square sections (HSS) with a nominal strength of 295 MPa. The measured material properties, yield strength σ_y, and ultimate strength σ_u are 330 MPa and 426 MPa for the first-story column and 332 MPa and 419 MPa for the rest of the columns. The wide flange beams of the test structure range from 340 to 400mm in depth and have nominal yield strength of 235 MPa.The predominant periods of the test structure ard 0.80 and 0.76 s in the X- and Y-directions according to the 3D white noise tests, respectively [19].

This full-scale structure was tested in 2007 at the Japanese E-Defense three-dimensional shaking table facility, which includes the world's largest shaking table of 20 by 15 m in plan view. The loading protocol for dynamic shaking of the test structure consisted of progressively increased ground motion intensities of the JR Takatori ground motion recorded during the 1995 M_w 6.9 Kobe earthquake [19]. All three components (two horizontal and one vertical) of this ground motion were applied simultaneously. The east-west (EW) component was assigned to the Y-direction of the structure, and the north-south (NS) component was assigned to the X-direction. The EW component of the ground motion was the strongest (PGA of 0.67 g) and caused dominated structure damage [19]. During the shaking table test, the structure was subjected to a sequence of 20 (Level 1), 40 (Level 2), 60 (Level 3), and 100% (Level 4) of the original JR Takatori ground motion records. The testing results show that the structure behaved elastically during the Level I (20%) shaking, with the peak inter-story drift ratios (θ) less than 0.05% (see Fig. 4). During the Level 2 (40%) shaking, the structure started to yield at the base, and the θ of the first and second stories reached 1.1%. During the 60% (Level 3) shaking, the θ of the first-story reached about 1.9%, and the θ of the upper stories progressively decreased, indicating an overall multi-story sideway yielding mechanism. During the 100% (Level 4) shaking, the θ of the first story reached 18.8%, and the structure collapsed with a first-story sideway mechanism (see Fig. 3(c)). The elapsed time until the complete collapse was 6.57 s. Detailed information regarding the testing protocol and test results can be found in [19][20].

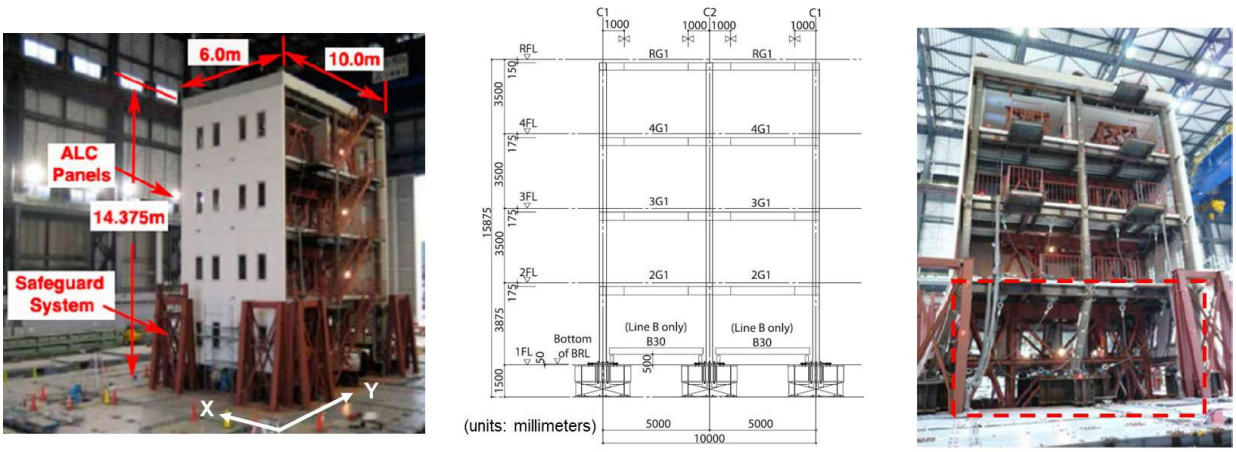

(a) (b) (c)

Fig. 3 The selected 4-story steel structure: (a) test setup on the E-Defense shaking table; (b) view in the Y direction; and (c) first-story collapse mechanism (modified from [19])

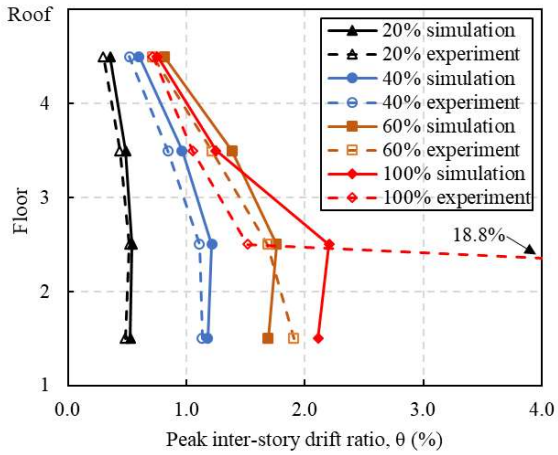

Fig. 4 Peak inter-story drift ratio distribution from the shaking table experiment and the numerical simulation

4. Numerical model and validation

Although the full-scale shaking table tests described in Section 2 provide the most reliable way to characterize the seismic behavior of the structure, its extraordinary expenses impede the probabilistic analysis and the evaluation of the effects of different input ground motion types of the seismic performance of structures. Numerical simulation provides a more cost-effective way to study the seismic response of the structure. Many available numerical models are capable of predicting the seismic response of the selected steel structure during design level earthquakes and near collapse [21][22]. This study selects the two-dimensional numerical model implemented by Lignos et al. [19] with the Open System for Earthquake Engineering Simulation (OpenSees) platform [23] since it shows acceptable accuracy and computation efficiency for the following probabilistic analysis. The numerical model is downloaded from the DesignSafe website [https://www.designsafe-ci.org/data/browser/public/].

The two-dimensional numerical model of [19] only characterizes the Y-direction geometry of the selected structure (see Fig. 5(a)). The P-Δ effect was considered using the corotational transformation, and the component deterioration was considered using the modified Ibarra-Medina-Krawinkler model [24],[25]. The steel beams and columns were modeled with elastic beam-column elements and concentrated plasticity rotational springs at their ends (see Fig. 5(a)). These springs followed a bilinear hysteretic response and included deterioration based on the modified Ibarra-Medina-Krawinkler deterioration model (see Fig. 5(b)). The material parameters were calibrated from the shaking table experiment [19]. To assess the seismic response of the steel structure, we applied the scaled intensities (20, 40, 60, and 100%) of the JR Takatori record sequentially to the developed numerical model. The simulated peak inter-story drift ratios are shown in Fig. 4 together with the experimental results. The comparison shows that the numerical simulations match well with experimental results, especially for the 20, 40, and 60% input ground motions. It is noted here that the numerical model does not converge during the 100% shaking input due to the structure collapse, and the data shown in Fig. 4(b) is the peak inter-story drift ratio recorded before the structure collapse. The collapse occurrence time is predicted slightly later (t=6.7 s) compared with the experimental result (t=6.57 s).

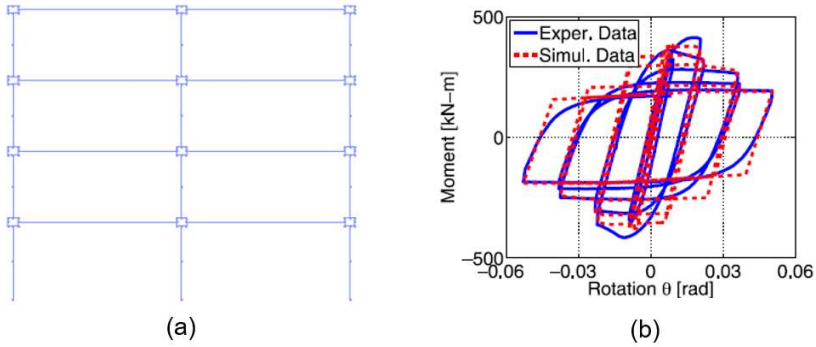

Fig. 5 The numerical model of the selected structure: (a) OpenSees model geometry; and (b) calibrated hysteretic responses of the modified Ibarra-Medina-Krawinkler deterioration model (from [19])

5. Seismic fragility analysis and liquefaction effect evaluation

5.1 Fragility curve

The seismic fragility curve is one key element of probabilistic seismic performance. The fragility curve describes the conditional probability, i.e., the likelihood of a structure exceeding a specific damage level for a given hazard intensity (see Eq. (1)).

$$P_f(x) = P(DM > ds \mid IM = x) \tag{1}$$

where *DM* is the damage measure of the structure or structural component, such as displacement, strain, ductility, and acceleration; *IM* is the hazard intensity measure, such as PGA and PSA; x is the realized condition of the hazard intensity measure *IM*; and *ds* is the threshold *DM* value for a specific damage level.

In practice, the damage measure and structural capacity parameters are assumed as random variables with lognormal distribution, and the fragility is also a lognormal distribution function [26]. Eq. (1) becomes:

$$P_f(x) = \Phi\left(\frac{\ln x - \mu}{\sigma}\right) \tag{2}$$

where $\Phi(\bullet)$ denotes the cumulative distribution function of the standard normal distribution; μ and σ are the median and standard deviation of the lognormal distribution function needed to describe the fragility curve, respectively.

Analytical methods are commonly used to produce a dataset for fragility curve development. [26] reviewed the four main methods used for deriving analytical fragility curves: the safety factor method, regression analysis, maximum likelihood estimation, and incremental dynamic analysis (IDA) method. In this work, IDA is used to develop the seismic fragility curves of the building described in Section 2. It is used to investigate the effects of different types of input ground motions on seismic fragility curves. IDA is based on nonlinear structural dynamic analyses utilizing a set of accelerograms scaled to the same shaking intensity level [27]. Ideally, the numerical structure model will behave from elastically and transition through an inelastic state to collapse with the gradual increment of *IM*. The most common seismic *IMs* are the Peak Ground Acceleration (PGA) and the Pseudo Spectral Acceleration (PSA) value at the fundamental period of the structure [26]. The PGA is selected as the *IM* here. The 344 ground motions mentioned in Section 2 are scaled to 30 levels of PGA. The *IM* values are selected from 0.05g to 1.0 g with an increment of 0.05 g and from 1.1g to 2.0 g with an increment of 0.1 g. The smaller increment used in the lower PGA range is to better capture the transition from linear to nonlinear structure dynamic response. The larger increment step in the larger PGA range is to reduce the computation efforts as the selected building is likely to collapse when the PGA exceeds 1 g. The numerical model described in Section 4 is tested with the input ground motion

from all combinations of the 344 raw records described in Section 2 and the 30 levels of scaling described previously. Hence, we run the numerical model 344×30 = 10,020 times on Clemson University's high-performance computing (HPC) resource [https://www.palmetto.clemson.edu/palmetto/]. The numerical simulation tool is the OpenSees (version 2.5.0).

After the nonlinear time history analyses, we need to select damage measures to define the damage state. Usually, the peak floor accelerations are correlated with nonstructural components' damage, while the maximum peak inter-story drift ratio correlates well with the structural damage states [28]. Hence, our *DM* is selected as the maximum peak inter-story drift ratio (termed as $\theta_{\max}$), which is defined as the maximum over time and overall stories of the inter-story drift ratios recorded during the time-history analysis. For this study, we choose to use two damage states: immediate occupancy (IO) and collapse (CO). For a steel moment-resisting frame, IO is violated when the maximum inter-story drift ratio reaches 0.7%, according to ATC 58-2 [29]. CO happens when the numerical model does not converge due to exceedingly large $\theta_{\max}$. The IDA curves plot the damage measures (here $\theta_{\max}$) with the intensity measure (here PGA) of the same structural model under different accelerograms parameterized on the same *IM*s [27] (see Fig. 6). The probability of exceedance of each damage state is determined by dividing the number of IDA curves that reached or exceeded the specified damage state by the total number of IDA curves. Then the lognormal distribution fitting is applied to obtain the fragility curves of the specific damage states. Here, we demonstrate the process of deriving the fragility curve for the collapse state using all the accelerograms. $\theta_{\max}$ generally increases with the increment of PGA on each IDA curve. When the IDA curve stops rising at a specific PGA level, it means that the building collapses at the next PGA level, where no $\theta_{\max}$ is derived from the time history analysis using this scaled accelerogram. For each PGA level, we can calculate $P_f(x)$ as the ratio of the number of accelerograms that cause building collapse to the total number of accelerograms. We take the PGA of 2.0 g as an example. If the IDA curve reaches the highest PGA level used in this study (i.e., 2 g), it means the structure does not collapse even when the PGA of this accelerogram is scaled to 2 g. Four accelerograms, approximately 98% of the total accelerograms, do not cause building collapse when their PGA are scaled to 2 g (see Fig. 6). We conduct such calculations for each PGA level and get the $P_f(x)$ values corresponding to PGA values shown in Fig. 7. The fitting to lognormal distribution function is then performed to obtain the fragility curve for the collapse state (see Fig. 7), as well as its fitting parameters (μ and σ).

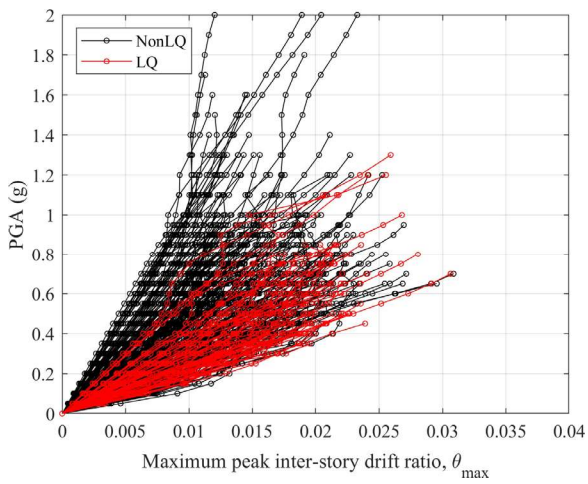

Fig. 6 The IDA curve sets

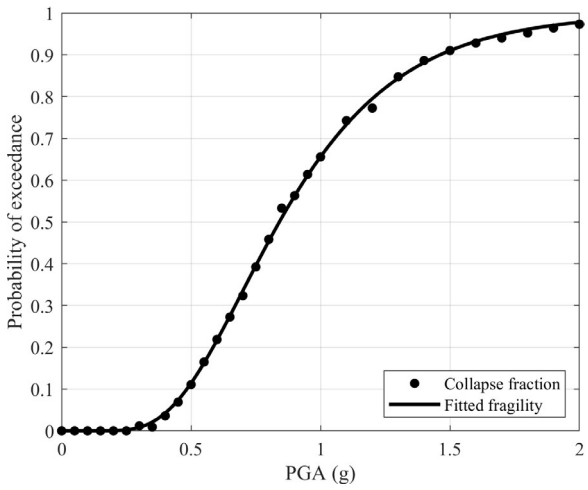

Fig. 7 Fragility curve demonstration

5.2 Liquefaction effects on seismic fragility curves

Three types of fragility curves are developed using the identical procedure described previously to evaluate the influence of liquefaction-modified ground motions on the fragility curves. They are based on liquefaction-modified accelerograms, non-liquefaction-modified accelerograms, and a combination of liquefaction-modified and non-liquefaction-modified accelerograms. Fig. 8 presents the fragility curves for the IO and CO damage states for the three types of ground motions, respectively. Each curve is assumed to be a cumulative distribution function for a lognormal distribution given the intensity measure (PGA) values shown in the horizontal axis. The two parameters for the fragility curves, median and standard deviation values, are listed in Tab. 1. The results show that the liquefaction-modified fragility curves generally have larger probability values than the non-liquefaction-modified fragility curves given the same PGA values, which indicates the selected structure is more vulnerable to the liquefaction-modified ground motions. Fig. 6 shows the θ_{max} demand parameters versus PGA for different groups of ground motion records. The results also show that given the same PGA level, the liquefaction-modified ground motions tend to generate larger θ_{max} than the non-liquefaction-modified ground motions.

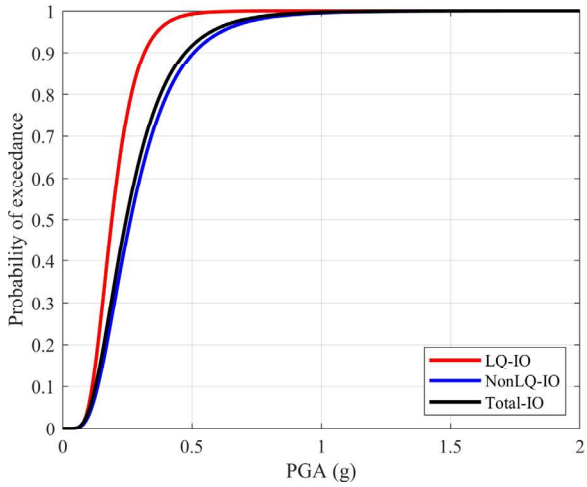

(a) Immediate Occupancy

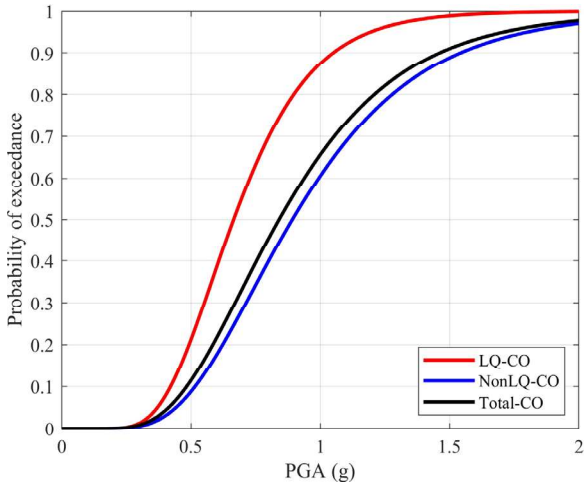

(b) Collapse

Fig. 8 Collapse fragility curves for different types of ground motion records: (a) violating immediate occupancy (IO) damage state; and (b) collapse (CO) damage state

Tab. 1 Fragility curve parameters for liquefaction-modified and non-liquefaction-modified ground motion records

PGA (g)	IO		CO	
	μ	σ	μ	σ
LQ	-1.659	0.395	-0.408	0.356
NonLQ	-1.338	0.514	-0.114	0.427
Total	-1.404	0.513	-0.173	0.432

To quantitatively evaluate the liquefaction effects on the fragility curve in terms of modifying the input ground motions for dynamic structural analysis, we compute the amplification ratio between the damage probability values using the fragility curves of LQ and NonLQ ground motions for the two damage states and every PGA levels (see Fig. 9). The amplification ratio larger than one means that liquefaction has an amplification effect on the collapse probability and vice versa. The results suggest that the amplification effects of liquefaction on building fragility are dependent on the damage state and PGA level. Liquefaction tends to amplify the probability of exceeding the immediate occupancy (IO) state for the PGA range of 0.07g~0.8g where the average amplification ratio is about 1.3. The amplification ratio for IO state peaks at PGA of 0.14g, and the peak amplification ratio is 2.0. As for the collapse (CO) state, liquefaction tends to amplify the probability of exceedance for the PGA range of 0.15g~2.0g where the average amplification ratio is about 1.5. The amplification ratio for the CO state peaks at a PGA of 0.4 g, and the peak amplification ratio is 2.5. The results indicate a strong adverse effect of liquefaction on the immediate occupancy violation and collapse probability of the selected building. The potential cause is that liquefaction can modify the ground motion' frequency component towards adversely impacting the structure's seismic response. The averaged pseudo-spectral acceleration value at the predominant period of the structure (0.76s) of the LQ ground motions are 0.69 g, which is about 1.7 times higher than that of the NonLQ ground motions (i.e., about 0.4 g) (see Fig. 2).

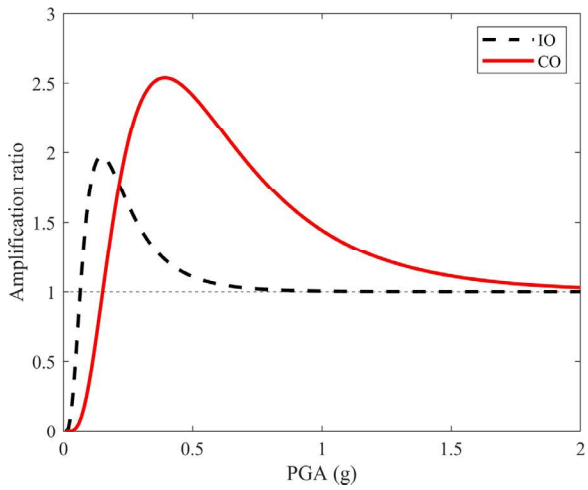

Fig. 9 Amplification ratio of the fragility curves due to liquefaction-modification effects on ground motions

6. Summary and Conclusion

Earthquake-induced soil liquefaction generated two types of demands on the structure: excessive ground deformation and modified ground motion. To advance the performance-based earthquake engineering practices at liquefiable sites, we proposed a framework for quantifying the effects of liquefaction-modified ground motions on the seismic fragility of building structures. A four-story steel moment-resisting frame structure used in the 2007 E-Defense full-scale shaking table test was selected as a case building. Incremental dynamic analyses were conducted to determine the seismic fragility curves of the case building

subjected to 344 ground motion records that belonged to three groups, liquefaction-modified accelerograms, non-liquefaction modified accelerograms, and all the accelerograms. The results suggest that the liquefaction could amplify the probability of exceeding collapse and immediate occupancy damage states by up to 2.5 and 2 times, respectively. This amplification effects of liquefaction-modified ground motions on building fragility are dependent on the damage state and PGA level. The cause of adverse effects of liquefaction on structure fragility is the enhancement of long-period ground motion components because liquefaction-induced soil softening allows more long-period ground motions to propagate to the ground. Future studies will need to explore such liquefaction effects using different building types and other intensity measures such as pseudo-spectral acceleration and peak ground velocity.

7. References

[1] Bird JF, Bommer JJ (2004): Evaluating earthquake losses due to ground failure and identifying their relative contribution. *Thirteenth World Conference on Earthquake Engineering (13WCEE)*, Vancouver, Canada.

[2] Cox BR, Boulanger RW, Tokimatsu K, Wood CM, Abe A, Ashford S, Donahue J, Ishihara K, Kayen R, Katsumata K, Kishida T (2013). Liquefaction at strong motion stations and in Urayasu City during the 2011 Tohoku-Oki earthquake. *Earthquake Spectra*, 29(1_suppl), 55-80.

[3] Cubrinovski M, Taylor M, Henderson D, Winkley A, Haskell J, Bradley BA, Hughes M, Wotherspoon L, Bray J. and O'Rourke T. (2014): Key factors in the liquefaction-induced damage to buildings and infrastructure in Christchurch: Preliminary findings. *2014 New Zealand Society for Earthquake Engineering (NZSEE) Annual Technical Conference*, Auckland, New Zealand.

[4] Maurer BW, Green RA, Cubrinovski M, Bradley BA (2014): Evaluation of the liquefaction potential index for assessing liquefaction hazard in Christchurch, New Zealand. *Journal of Geotechnical and Geoenvironmental Engineering*, 140(7):04014032.

[5] Van Ballegooy S, Malan P, Lacrosse V, Jacka ME, Cubrinovski M, Bray JD, O'Rourke TD, Crawford SA, Cowan H (2014): Assessment of liquefaction-induced land damage for residential Christchurch. *Earthquake Spectra*, 30(1):31-55.

[6] Bray JD, Macedo J (2017): 6th Ishihara lecture: Simplified procedure for estimating liquefaction-induced building settlement. *Soil Dynamics and Earthquake Engineering*, 102, 215-231.

[7] Ishihara K, Yoshimine M (1992): Evaluation of settlements in sand deposits following liquefaction during earthquakes. *Soils and foundations*, 32(1):173-188.

[8] Holzer TL, Hanks TC, Youd TL (1989): Dynamics of liquefaction during the 1987 Superstition Hills, California, earthquake. *Science*, 244(4900):56-59.

[9] Iai S, Morita T, Kameoka T, Matsunaga Y, Abiko K (1995): Response of a dense sand deposit during 1993 Kushiro-Oki Earthquake. *Soils and foundations*, 35(1):115-131.

[10] Bonilla LF, Archuleta RJ, Lavallée D (2005): Hysteretic and dilatant behavior of cohesionless soils and their effects on nonlinear site response: Field data observations and modeling. *Bulletin of the Seismological Society of America*, 95(6):2373-2395.

[11] Roten D, Fäh D, Bonilla LF (2013): High-frequency ground motion amplification during the 2011 Tohoku earthquake explained by soil dilatancy. *Geophysical Journal International*, 193(2):898-904.

[12] Youd TL, Carter BL (2005): Influence of soil softening and liquefaction on spectral acceleration. *Journal of Geotechnical and Geoenvironmental Engineering*, 131(7):811-825.

[13] Gingery JR, Elgamal A, Bray JD (2015): Response spectra at liquefaction sites during shallow crustal earthquakes. *Earthquake Spectra*, 31(4):2325-2349.

[14] Zhan W, Chen Q (2021): An accelerogram-based method for quick assessment of liquefaction occurrence. *Journal of Geotechnical and Geoenvironmental Engineering* (accepted)

[15] Zhan W (2020): Data-Driven Assessment of Site Responses at Liquefiable Sites. Ph.D. dissertation, Clemson University, Clemson, USA.

[16] Kostadinov MV, Yamazaki F (2001): Detection of soil liquefaction from strong motion records. *Earthquake engineering & structural dynamics*, 30(2):173-93.

[17] Architectural Institute of Japan (AIJ) (2006): Report of seismic performance improvement of civil, architectural structures subjected to long-period ground motions generated by subduction zone. *Report of Japan Society of Civil Engineering*, Tokyo (in Japanese).

[18] Building Center of Japan (BCJ) (2008): *Building standard law of Japan*, BCJ, Tokyo.

[19] Lignos DG, Hikino T, Matsuoka Y, Nakashima M (2013): Collapse assessment of steel moment frames based on E-Defense full-scale shake table collapse tests. *Journal of Structural Engineering*, 139(1):120-32.

[20] Suita K, Yamada S, Tada M, Kasai K, Matsuoka Y, Shimada Y (2008): Collapse experiment on 4-story steel moment frame: Part 2 detail of collapse behavior. *Proceedings of the 14th world conference on earthquake engineering*, Beijing, China.

[21] Ohsaki M, Kasai K, Hikino T, Matsuoka Y (2008). Overview of 2007 E-Defense blind analysis contest results. *Proceedings of the 14th world conference on earthquake engineering*, Beijing, China.

[22] Ohsaki M, Kasai K, Thiagarajan G, Yang Y, Komiya Y (2008): 3-D analysis methods for 2007 blind analysis contest. Proceedings of the 14th world conference on earthquake engineering, Beijing, China.

[23] McKenna FT (1997): Object-oriented finite element programming: Frameworks for analysis, algorithms and parallel computing. Ph.D. Dissertation, Univ. of California-Berkeley, Berkeley, CA.

[24] Ibarra LF, Medina RA, Krawinkler H (2005): Hysteretic models that incorporate strength and stiffness deterioration. *Earthquake engineering & structural dynamics*, 34(12):1489-1511.

[25] Lignos, DG, Krawinkler H (2009): Sideway collapse of deteriorating structural systems under seismic excitations. *Rep. No. TR 172*, John A. Blume Earthquake Engineering Center, Dept. of Civil Engineering, Stanford Univ., Stanford, CA.

[26] Zentner I, Gündel M, Bonfils N (2017): Fragility analysis methods: Review of existing approaches and application. *Nuclear Engineering and Design*, 323:245-258.

[27] Vamvatsikos D, Cornell CA (2002): Incremental dynamic analysis. *Earthquake Engineering & Structural Dynamics*, **31** (3), 491-514.

[28] Vamvatsikos D, Cornell CA (2004): Applied incremental dynamic analysis. *Earthquake Spectra*, 20(2):523-553.

[29] ATC 58–2 (2003): Preliminary Evaluation of Methods for Defining Performance. Report ATC 58-2, Applied Technology Council, Redwood City, CA (available at http://www. atcouncil.org/pdfs/ATC582.pdf).

